**Supplementary Methods**
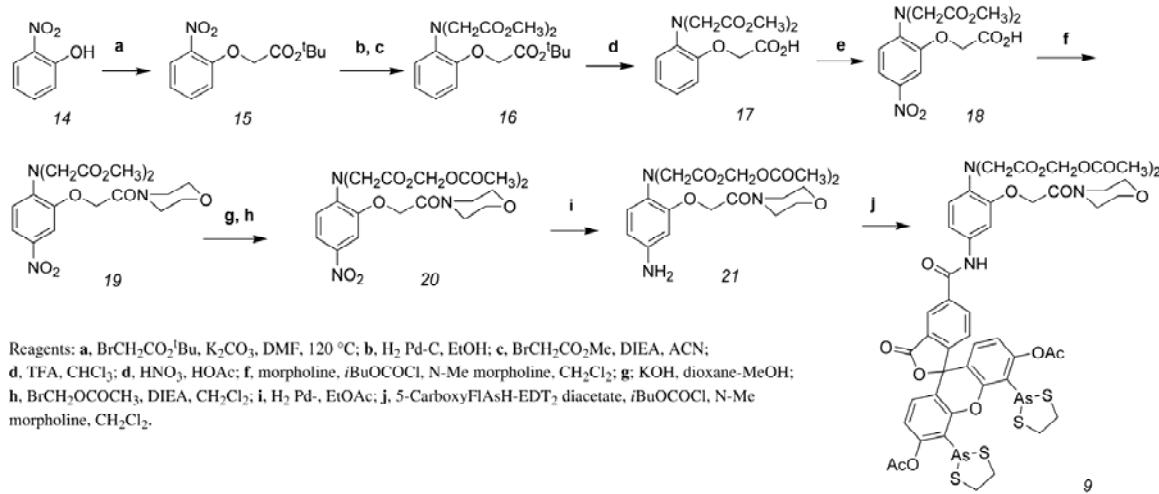
**Synthesis of Calcium-Green-FlAsH.** Structures of compounds are presented in the figure below.



Reagents: **a**, BrCH$_2$CO$_2$$^t$Bu, K$_2$CO$_3$, DMF, 120 °C; **b**, H$_2$ Pd-C, EtOH; **c**, BrCH$_2$CO$_2$Me, DIEA, ACN; **d**, TFA, CHCl$_3$; **d**, HNO$_3$, HOAc; **f**, morpholine, $i$BuOCOCl, N-Me morpholine, CH$_2$Cl$_2$; **g**; KOH, dioxane-MeOH; **h**, BrCH$_2$OCOCH$_3$, DIEA, CH$_2$Cl$_2$; **i**, H$_2$ Pd-, EtOAc; **j**, 5-CarboxyFlAsH-EDT$_2$ diacetate, $i$BuOCOCl, N-Me morpholine, CH$_2$Cl$_2$.

Materials and instrumentation were as previously described (Adams et al, 2002, ref. 27) except electrospray mass spectroscopy was performed using a Agilent Iontrap (Santa Clara, CA) and $^{13}$C NMR spectra were obtained on a Bruker DRX-600 spectrometer (Billerica, MA).

*t-Butyl 2-nitrophenoxyacetate (**15**):* 2-Nitrophenol (**14**), (85%, 4.1 g, 25 mmol) was dissolved in dry DMF (25 mL) with dry K$_2$CO$_3$ and heated at 120 °C under N$_2$ until all gas was evolved. t-Butyl bromoacetate (4.44 mL, 27.5 mmol) was added causing the mixture to turn pale orange from a deep red. After 10 mins, the reaction was cooled and diluted with H$_2$O and saturated NaHCO$_3$ and extracted (3 x 50 mL) with toluene. After drying over Na$_2$SO$_4$, the extract was evaporated to an oil which was distilled by kugelrohr (50 µm Hg, 110 °C) to give the product as a pale yellow oil. Yield, 6.35 g (100%).

$^1$H-NMR: δ (200 MHz, CDCl$_3$, ppm) 1.47 (s, 9H, t-Bu), 4.67 (s, 2H, O-CH$_2$-), 6.97 (dd, 1H, J=15, 1.7 Hz, H-6), 7.08 (m, 1H, H-5), 7.52 (m, 1H, H-4), 7.87 (dd, 1H, J=15, 2.6Hz, H-3). ES-MS; +ve mode (M+1)$^+$ 254.1, (M+Na$^+$) 276.0. Calc'd for [C$_{12}$H$_{15}$NO$_5$ + H$^+$] ; 254.1.

*t-Butyl N,N-bis(methoxycarbonymethyl)2-aminophenoxyacetate (**16**):* t-Butyl 2-nitrophenoxyacetate (2.5 g, 10 mmol) was dissolved in 95% EtOH (25 mL) with Pd-C and hydrogenated at room temperature and pressure. After filtration and evaporation of the solvent, the resulting amine was dissolved in dry $CH_3CN$ with methyl 2-bromoacetate (2.84 mL, 30 mmol) and di-isopropylethylamine (5.23 mL, 30mmol) and the resulting solution was refluxed overnight under argon. The reaction mixture was cooled, diluted with toluene (50 mL) , filtered to remove salt and washed with 1 M-phosphate buffer pH 2 (2 x 30 mL) and $H_2O$ (30 mL). After drying ($Na_2SO_4$), the solution was evaporated to dryness and distilled (50 μm Hg, 150 °C) to yield the product as a yellow oil. Yield, 3.1 g (84 %).

^{1}H-NMR: δ (200 MHz, $CDCl_3$, ppm) 1.47 (s, 9H, t-Bu), 3.72 (s, 6H, Me), 4.22 (s, 4H, N-$CH_2$-), 4.52 (s, 2H, O-$CH_2$-), 6.75-6.9 (m, 4H, aromatic). ES-MS; +ve mode (M+1)$^+$ 368.1. Calc'd for $[C_{18}H_{25}NO_7 + H^+]$ ; 368.2.


*N,N-2-Bis(methoxycarbonylmethyl)aminophenoxyacetic acid (**17**):* **16** 100 mg, 0.27 mmol) was treated with 25 % trifluoroacetic acid -$CHCl_3$ (1 mL) at room temperature overnight under $N_2$, evaporated and diluted with $CHCl_3$ (25 mL). The product was extracted into aq. $NaHCO_3$ (3 x 20 mL), precipitated upon acidification with HOAc and extracted with EtOAc (3 x 20 mL). After drying ($Na_2SO_4$), the crude product was obtained as a colorless oil. Yield, 85 mg (100%).

^{1}H-NMR: δ (200 MHz, $CDCl_3$, ppm) 3.73 (s, 6H, Me), 4.14 (s, 4H, N-$CH_2$), 4.71 (s, 2H, O-$CH_2$), 6.9-7.1 (m, 4H, aromatic). ES-MS; +ve mode (M+1)$^+$ 312.1. Calc'd for $[C_{14}H_{17}NO_7 + H^+]$ ; 312.1.


*N,N-2-Bis(methoxycarbonylmethyl)amino-5-nitrophenoxyacetic acid (**18**):* **17** (311 mg, 1 mmol) was dissolved in acetic acid (1 mL) at room temperature with sodium nitrite (7 mg, 0.1mmol) and 70 % nitric acid (70 μL, 1.1 mmol) was added in 5 μL portions with stirring. The reaction mixture was poured into water (25 mL) and extracted with EtOAc

(3 x 20 mL). After drying (Na$_2$SO$_4$), evaporation, and trituration with EtOH gave the product as a yellow solid, 158 mg (44%).

$^1$H-NMR:  δ (200 MHz, CDCl$_3$, ppm) 3.78 (s, 6H, Me), 4.26 (s, 4H, N-CH$_2$), 4.71 (s, 2H, O-CH$_2$), 6.77 (d, 1H, H-3, J=8.9Hz), 7.68 (d, 1H, H-6, J=2.4Hz), 7.88 (dd, 1H, H-4, J=2.4, 8.9Hz). ES-MS; +ve mode (M+1)$^+$ 357.0. Calc'd for [C$_{14}$H$_{16}$N$_2$O$_9$ + H$^+$] ; 357.1.


*N-(N',N'-2-bis(methoxycarbonylmethyl)amino-5-nitrophenoxyacetyl)-morpholine* **(19):**
**18** (142 mg, 0.4 mmol)  and  N-methylmorpholine (57 µL, 0.52 mmol) dissolved in dry CHCl$_3$ under Ar at 0 °C, was treated with isobutylchloroformate (62 µL, 0.48 mmol). After 20 mins, morpholine (42 µL, 0.48 mmol) was added, the reaction mixture was allowed to warm to room temperature, stirred for 30 min and diluted with EtOAc (20 mL) and washed with 1M-phosphate buffer pH 2 (3 x 10 mL). After drying (Na$_2$SO$_4$), evaporation and trituration with cold EtOH, the product was obtained as a yellow solid, 130 mg (76%).

$^1$H-NMR:  δ (200 MHz, CDCl$_3$, ppm) 3.5-3.7 (br m, 8H, morpholine), 3.78 (s, 6H, Me), 4.29 (s, 4H, N-CH$_2$), 4.76 (s, 2H, O-CH$_2$), 6.75 (d, 1H, H-3, J=9.2Hz), 7.67 (d, 1H, H-6, J=2.5Hz), 7.86 (dd, 1H, H-4, J=2.5, 9.2Hz) . ES-MS; +ve mode (M+1)$^+$ 426.1. Calc'd for [C$_{18}$H$_{23}$N$_3$O$_9$ + H$^+$] ; 426.1.


*N-(N',N'-2-bis(acetoxymethoxycarbonylmethyl)amino-5-nitrophenoxyacetyl)-morpholine*
*(20):* **19** (85 mg, 0.2 mmol) was dissolved in dioxane-MeOH (1:1 v/v, 1mL) and treated with 1M-KOH (0.42 mL)  portionwise with stirring. After overnight reaction, the mixture was evaporated, dissolved in water (10 mL), acidified with 1M-HCl (0.42 ml) and a drop of HOAc, and extracted with EtOAc (5 x 20 ml). After drying (MgSO$_4$) and evaporation to a yellow foam (76 mg), the free acid was suspended in dry CH$_2$Cl$_2$ (2 mL) under Ar and treated with DIEA (140 µL, 0.8 mmol) and bromomethylacetate (83 µL, 0.8 mmol). After reaction overnight, the mixture was diluted with CHCl$_3$ (20 mL), washed with 1M phosphate buffer pH 2 (3 x 10 mL), dried and evaporated. The product was obtained as a yellow oil (67 mg, 63%) after separation on silica gel with ethyl acetate –hexanes (4:1 v/v).

$^1$H-NMR: δ (200 MHz, CDCl$_3$, ppm) 2.12 (s, 6H, Ac), 3.5-3.7 (br m, 8H, morpholine), 4.32 (s, 4H, N-CH$_2$), 4.80 (s, 2H, O-CH$_2$), 5.80 (s, 4H, O-CH$_2$-O), 6.73 (d, 1H, H-3, J=9.0Hz), 7.65 (d, 1H, H-6, J=2.5Hz), 7.83 (dd, 1H, H-4, J=2.5, 9.0Hz). ES-MS; +ve mode (M+1)$^+$ 542.1. Calc'd for [C$_{22}$H$_{27}$N$_3$O$_{13}$ + H$^+$] ; 542.2..

*N-(N',N'-2-bis(acetoxymethoxycarbonylmethyl)amino-5-aminophenoxyacetyl)-morpholine (21):* **20** (33 mg, 0.061 mmol) was hydrogenated over Pd-C at room temperature and pressure in EtOAc. Uptake was complete in one hour and the mixture was filtered through Celite and evaporated to give the product as a colorless oil (31 mg, 100%).

$^1$H-NMR: δ (200 MHz, CDCl$_3$, ppm) 2.08 (s, 6H, Ac), 3.5-3.7 (br m, 8H, morpholine), , 4.10 (s, 4H, N-CH$_2$), 4.72 (s, 2H, O-CH$_2$), 5.72 (s, 4H, O-CH$_2$-O), 6.73 (d, 1H, H-3, J=9.0Hz), 7.65 (d, 1H, H-6, J=2.5Hz), 7.83 (dd, 1H, H-4, J=2.5, 9.0Hz) ES-MS; +ve mode (M+1)$^+$ 512.2. Calc'd for [C$_{22}$H$_{29}$N$_3$O$_{11}$ + H$^+$] ; 512.2.

*5-carboxyFlAsH diacetate* (**22**), *4',5'-Bis(1,2,3-dithioarsolan-2-yl)-fluorescein-5-carboxylic acid diacetate:* 4',5'-Bis(1,2,3-dithioarsolan-2-yl)-fluorescein-5-carboxylic acid (30 mg, 0.042 mmol) was heated in HOAc-acetic anhydride (1:1 v/v 0.4 mL) with pyridine (20 µL) at 60°C for 3h. The colorless solution was evaporated and the residue triturated with 50% EtOH to give the product as a white solid, 30 mg (95%).

$^1$H-NMR: δ (200 MHz, CDCl$_3$, ppm) 2.37 (s, 6H, Ac), 3.3-3.7 (br m, 8H, S-CH$_2$-), 6.74, 6.75 (dd, 4H, xanthene), 7.93 (s, 1H, benzoic H-4), 8.10, 8.35 (2d, 2H, benzoic H-6,7). ES-MS; +ve mode (M+1)$^+$ 792.9. Calc'd for [C$_{29}$H$_{22}$As$_2$O$_9$ + H$^+$] ; 792.9.

*Calcium-Green-FlAsH diacetate bisacetoxymethyl ester (9):* 5-CarboxyFlAsH diacetate (**22**, 14.6 mg, 20 µmol) dissolved in dry CH$_2$Cl$_2$ under Ar at 0°C was treated with isobutylchloroformate (2.8 µL, 21.6 µmol) and then N-methylmorpholine (2.9 µL, 22.5 µmol) and the solution was stirred for 20 min. **8** (10 mg, 20 µmol) dissolved in minimum dry CH$_2$Cl$_2$ was added, and the reaction mix was allowed to warm to room temperature and kept overnight. After quenching with a few drops of HOAc, the reaction mix was diluted with CHCl$_3$ (20 mL), washed with water (x2) and dried (Na$_2$SO$_4$). The product

was obtained following separation on silica gel by elution with EtOAc, as a colorless gum, 5.1 mg (20%).

$^1$H-NMR: δ (200 MHz, CDCl$_3$, ppm) 2.10 (s, 6H, 3',6'-OAc), 2.37 (s, 6H, Ac) 3.3-3.7 (br m, 16H, morpholine and EDT), 4.19 (s, 4H, N-CH$_2$), 4.75 (s, 2H, O-CH$_2$), 5.75 (s, 4H, O-CH$_2$-O), 6.74, 6.93 (2d, 4H, xanthene J=8.6Hz), 6.87 (d, 1H, H-3, J=9Hz), 7.2 (d, 1H, H-6, J=2Hz), 7.3 (dd, 1H, H-4, J=2, 9.0Hz), 7.66 (s, 1H, benzoic H-4), 8.08, 8.17 (2d, 2H, benzoic H-6,7). $^{13}$C NMR (125 MHz, d$_6$-DMSO): δ 20.54, 21.45, 42.79, 43.02, 53.02, 59.82, 65.80, 65.90, 65.98, 66.04, 79.06, 81.52, 107.34, 114.08, 116.01, 118.62, 120.66, 122.69, 124,70, 125.70, 128.14, 129.62, 130.56, 132.75, 134.70, 141.54, 149.08, 151.09, 152.09, 152.96, 163.16, 165.79, 167.41, 169.35, 169.54, 169.79. LC-MS indicated partial loss of the phenolic acetate esters. ES-MS; +ve mode (M+1)$^+$ 1286.5. Calc'd for [C$_{51}$H$_{49}$As$_2$N$_3$O$_{19}$S$_4$ + H$^+$]; 1286.0

*CaG FlAsH complexes with tetracysteine peptides:* Calcium-Green-FlAsH diacetate AM ester (**9**) was added to a solution of tetracysteine peptide in 10 mM 2-mercaptoethanesulfonate 3 mM TCEP 10mM K-MOPS pH 7.2 containing pig liver esterase (Sigma) and kept at room temperature for 3-24 h. Reaction could be monitored by LC-MS e.g. the complex of CaG FlAsH with FLNCCPGCCMEP-NH$_2$ gave peak of 1093.4 in +ve mode. Calc'd for [C$_{90}$H$_{111}$As$_2$N$_{17}$O$_{30}$S$_5$ + 2H$^+$]; 1092.7.

*Calcium and magnesium titrations of CaGF:* Calcium titrations were measured in a cuvette by sequential addition of CaCl$_2$ solutions to a micromolar solution of CaGF complex with our original tetracysteine peptide dissolved in 100 mM KCl (Ultrex grade, Fisher) 10 mM K.MOPS pH 7.2. Hill plots of the resulting intensity changes against –log[Ca$^{2+}$] gave the dissociation constants as x intercepts. In the presence of 15 mM calcium, adding 1 mM BAL (2,3-dimercaptopropanol) removes the CaGF from the tetracysteine peptide resulting in a sharp decrease in CaGF fluorescence (unbound to peptide trace in Fig. 1b). Magnesium titrations were performed similarly giving a value of ~10 mM for the complex.

*Quantum yields of fluorescence and photobleach of CaGF:*  The fluorescence quantum yield of the CaGF complex with the peptide FLNCCPGCCMEP-NH$_2$ in saturating Ca$^{2+}$ was 0.57. Quantum yields of photodestruction were measured as previously described (Baird et al, 2000). Irradiation of microdroplets of the Ca$^{2+}$ complex of CaGF and peptide with 1.49 watt/cm$^2$ at 480 nm showed that the fluorescence was well fitted by a biexponential decay. 68% of the amplitude had a time constant of 0.089 s$^{-1}$, while the remaining 32% had a time constant of 0.016 s$^{-1}$. These two time constants correspond to photobleach quantum yields of 2.45 x 10$^{-4}$ and 4.36 x 10$^{-5}$ respectively.

**Stopped-flow.**  Experiments were performed on an Applied Photophysics (Surrey, U.K.) Stopped Flow. An equal volume of CaGF bound to excess FLNCCPGCCMEP (final concentration of 2 μM) in 100 mM KCl, 10 mM MOPS pH 7.2 with 100 μM CaCl2 was rapidly mixed with the same buffer but replacing the CaCl$_2$ with 1, 10 or 50 mM BAPTA tetrapotassium salt (Invitrogen, Carlsbad, CA). The fluorescence was monitored by using an excitation wavelength of 500 nm and an emission bandpass filter of HQ 530/30 nm (Chroma, Rockingham, VT). All fluorescent changes were complete within the dead time of the instrument (1.5 ms).

**Completeness of labeling of Cx43-GFP-4C by CaGF in cells.** Assuming that Ca$^{2+}$-saturated CaGF bound to the tetracysteine has the same absorbance spectrum ($\varepsilon = 7$ x 10$^4$ M$^{-1}$cm$^{-1}$ at 508 nm, 3.3 x 10$^4$ M$^{-1}$cm$^{-1}$ at 488 nm, and with a quantum yield of 0.57, one calculates that the Ca$^{2+}$-dependent increment in fluorescence should be ~40% of the basal fluorescence due to the simple sum of Emerald GFP plus Ca$^{2+}$-free CaGF. Fig. 1f shows the Ca$^{2+}$-dependent increment is actually about equal to the basal fluorescence, slightly greater than expected for 1 CaGF per GFP. A similar ratio was obtained for the N4-GFP-$\alpha_{1C}$ construct (not shown). A possible explanation for the higher-than-expected ratio is that the GFP may be somewhat quenched by fluorescence resonance energy transfer to the CaGF.

**Estimation of the channel open probability.** The open probability ($P_{open}$) was obtained by dividing the number of open channels ($n_{open}$) by the estimated number of N4-GFP-$\alpha_{1C}$ channels on the membrane ($N_{membrane}$).

**Finding $n_{open}$:** the calcium ensemble current (I) divided by the single channel current (i) gives the number of open channels. i is obtained by multiplying the driving force across the membrane ($\Delta V$) by the single channel conductance ($\gamma$). Thus, $n_{open} = I/(\Delta V * \gamma)$.

**Finding $N_{cell}$:** to estimate the number of channels on the membrane, $N_{membrane}$, we first estimated the total number of GFP tagged channels in a cell ($N_{cell}$) with a confocal microscope (Zeiss LSM 5LIVE, Thornwood, NY). Using identical microscope settings, we acquired a stack of slices from a cell as well as a stack of slices from a micro-bubble containing purified GFP at a known concentration (described below). We sampled both specimens at 0.3$\mu$m per slice (50-200 slices) using low laser power to avoid photobleaching. The confocal images were used to reconstruct the micro-bubble dimensions and obtain its volume ($V_{bubble}$). The number of GFP molecules in a micro-bubble $N_{GFP}$ is given by $N_{GFP} = [GFP] * V_{bubble} * N_{Av}$, where $N_{Av}$ is Avogadro's number ($\sim 6.022 \times 10^{23}$). We divided $N_{GFP}$ by the sum of all the fluorescent counts from the micro-bubble slices ($\sum F_{bubble}$) to get our calibration factor, $fN_{GFP}$, which quantifies the number of GFP molecules that give rise to a fluorescent count; $fN_{GFP} = N_{GFP}/\sum F_{bubble}$. The sum of all the fluorescent counts from a stack of slices from a cell is $\sum F_{cell}$. Finally, multiplying $\sum F_{cell}$ by our calibration factor $fN_{GFP}$ gives an estimate of the number of GFP molecules in a given cell; $\sum F_{cell} * fN_{GFP} = N_{cell}$. In bright cells with nice membrane localization of GFP, similar to those we recorded from electrically, we found $N_{cell} = 3.7 \pm 1.2$ million channels (mean $\pm$ standard deviation, n=7; minimum was 1.7 million and maximum was 5.2 million).

**Finding $N_{membrane}$:** We summed the fluorescence of the confocal images of slices of the cell $\sum ROI_{cell}$. Next, we traced and summed the membrane fluorescence

($\Sigma ROI_{membrane}$). In both cases, background fluorescence was subtracted using a portion of the image with no cell as a reference. The fraction of channels on the membrane, f $N_{membrane}$, is given by: $\Sigma ROI_{membrane}/\Sigma ROI_{cell}$. Finally, multiplying $N_{cell}$ by $fN_{membrane}$ gives an estimation of the number of channels on the membrane.

**Preparation of GFP micro-bubbles:** Aqueous droplets of 1μM purified GFP in PBS were formed under mineral oil on a coverslip. For reproducibility, it proved essential to vortex the oil with an aqueous buffer prior to introducing the purified protein. This procedure removed any traces of autoxidized or acidic contaminants. The final droplets were small enough (5–10 μm diameter) so that all the molecules saw the same incident intensity.

**Estimating $N_{cell}$ using a flow cytometer.** An alternative and independent method to estimate the number of N4-GFP-$\alpha_{1C}$ channels in a cell, $N_{cell}$, is to run tens of thousands of these cells through a flow cytometer (FACSVantage, San Jose, CA) and to use a set of fluorescent beads (Bangs Laboratories, Fishers, IN) with a known number of fluorophores as a fluorescent standard. Note again that we used a single cell cloned stable cell line for N4-GFP-$\alpha_{1C}$, which exhibit a smaller variability in protein expression then transient transfection. We also measured the magnitude of green autofluorescence in the parental cells lacking GFP and found it to be significantly smaller then the N4-GFP-$\alpha_{1C}$ cell line (786 compared to 30,000 fluorescent units, respectively). For more details see Martin et al., 2005 (reference 32).

We observed substantial variability in the population of GFP-labeled cells (with tails at $N_{cell}$ =200,000 and $N_{cell}$ =8,000,000 channels). This variability is much larger than we observed with confocal reconstructions. There are two explanations for this. First, FACS sorting measured the entire population as opposed to the relatively bright cells chosen for electrophysiology and confocal reconstruction. Second, there are a variety of sources of noise specific to FACS sorting, including higher photon shot noise from the brief illumination, cell clumping, and nonuniform illumination of the sample, that could increase the spread of FACS measurements.

**Upper and Lower Bounds on $P_{open}$.** If we take the full range for $N_{cell}$ measured by FACS sorting, a typical measured value of 30% for the fraction of channels on the plasma membrane, and a typical measured current of 2500 pA for the current, the estimate for $P_{open}$ ranges from 6.7% to 0.17%, for the dimmest and brightest cells, respectively. However, this calculation is likely to be misleading, as we did not record from cells of all intensities, and FACS may overstate the variability in intensity. When we did attempt to record from particularly dim cells, the currents ranged from being buried within the noise to about 200 pA. Thus, the upper value for $P_{open}$ (for dim cells) is around 0.5%. Using the more reliable confocal data, and taking into account variability in currents and uncertainty in the fraction of channels on the surface, we find 0.1-0.3% as the best estimate of the range for $P_{open}$. In all cases the conclusion is the same: only a very small fraction of channels are open during depolarization; a more accurate quantitative measure would require confocal reconstruction and electrophysiology on the same cell.

**Finite Difference Models.** Finite difference models of extracellular calcium diffusion and intracellular calcium diffusion near a single channel were constructed using typical methods, similar to those described in (Shuai and Parker, 2005; reference 41). In brief, the model space was subdivided into a coarse grid of cubical elements with additional subdivision into a fine grid near areas of large concentration gradients. Diffusion between elements i and j sharing a common face was implemented as concentration updates of $\Delta C_i = -(1/V_i)*D*((C_i-C_j)/L_{ij})*A_{ij}*\Delta t$, where $C_i$ is the concentration in one element, D is the diffusion constant of the diffusing molecule, $V_i$ is the volume of the element, $A_{ij}$ is the area of the shared face, and $L_{ij}$ is the distance between centers of the two elements; this is simply a direct application of Fick's first law of diffusion. Unimolecular reactions were implemented as concentration updates $\Delta C_i = -k*C_i*\Delta t$, where k is the rate constant; products were updated with opposite sign. Bimolecular reactions were computed as $\Delta B_i = \Delta C_i = -k*B_i*C_i*\Delta t$, where $B_i$ is the other reactant; product concentrations were updated with the opposite sign. Concentration updates were calculated for the whole simulation and then applied at the end of each time step.

Extracellular depletion of calcium was modeled in a gap of 25, 50, or 100 nm under a 14 x 14 micron square that represented the cell body. The edges of the gap were clamped at the extracellular calcium concentration (15 mM) and calcium was extracted from the cellular face of the gap as if 1/3 of the current entering the entire cell were entering along the bottom face of the cell. The value of 1/3 was obtained from confocal reconstructions that showed that approximately 1/3 of the cell membrane is on the bottom face and accessible to TIRF microscopy; we assumed that the fractional current entry was equal to the fractional membrane area, that is, that the distribution of active channels was the same over the entire cell surface. We simulated a 20 ms pulse of 2 nA calcium current initially uniformly distributed over the cell. The current was adjusted using a phenomenological relationship for $g_{Ca}$ reported in Church & Stanley (1996; reference 38): $g_{Ca}=9.2/(1+5.6/[Ca])$ where the units of $g_{Ca}$ are pS and the constant 5.6 has units of mM. We implemented this equation in fractional form: $g_{Ca}/g_{Ca,initial}=[Ca]*([Ca]_{initial}+5.6)$ / $[Ca]_{initial}*([Ca]+5.6)$. We altered the driving force linearly with concentration, as the Goldman-Hodgkin-Katz current equation is nearly linear in extracellular concentration at +20 mV given a measured +110 mV reversal potential. Assuming no change in driving force, or a logarithmic change (Nernst equation), gave qualitatively similar results (data not shown). The extracellular calcium diffusion constant was assumed to be 600 $\mu m^2$/s. A 30x30x5 grid was used for each gap distance, where the grid element height was scaled to give five elements across the gap. Only one quarter of the system was modeled with boundary conditions adjusted to reflect the symmetry of the problem. We found that even with the smallest gap of 25 nm and at locations which are 7 $\mu m$ from the edge of the cell, the external calcium concentration decreased from 15 mM to ~12 mM. With larger gaps or locations closer to the cell edge, the depletion was much smaller. We therefore neglected the depletion effect for the rest of the simulations. Analysis of the fluorescence changes in images showed only a very weak negative correlation with intensity (R=-0.1 over a cell tiled with 1 $\mu m$ diameter spots, data taken from Supplementary Movie 1), while intensity should vary strongly with distance with TIRF imaging. This confirms that the distance between cover slip and cell surface has a minimal impact on calcium influx,

and in particular is consistent with simulation results indicating that extracellular calcium depletion is not a major factor.

Calcium diffusion around a channel was modeled in a 0.77 x 0.77 x 3.0 $\mu m^3$ box either with reflective sides (i.e. assuming a unit cell) and the top clamped at pre-stimulus concentrations to reflect access to the open pipette filled with buffer. Making the top face reflective made an essentially insignificant difference (not shown). CaGF was placed only in the grid elements closest to the membrane. Calcium was injected at the center of the membrane face of the box at the rate expected from a 7 pS channel with 100 mV of driving force. Coarse grid spacing of 20 nm was used farther than 40 nm from the channel, while a fine grid of 4 nm was applied closer than 40 nm to the channel. We used the following diffusion constants: calcium, 220 $\mu m^2$/s; EGTA, 113 $\mu m^2$/s; BAPTA, 95 $\mu m^2$/s (Smith, 2001). Buffer kinetics were: EGTA, $k_+$ = 2.7/$\mu$M/s, $k_-$=0.5/s; BAPTA, $k_+$=450/$\mu$M/s, $k_-$=80/s; CaGF, $k_+$ 750/$\mu$M/s, $k_-$=45000/s (values estimated from similar calcium binding moieties); immobile endogenous buffer, $k_+$ 2.7/$\mu$M/s, $k_-$=9/s (similar to Calbindin).

Calcium diffusion around a cluster of channels was modeled in a box 3 $\mu$m tall and with the lower face with an area of 0.6 $\mu m^2$ per channel (assuming 2500 active channels on a cell with 1500 $\mu m^2$ surface area). The grid was refined at least 5-fold in each dimension close to the source of calcium, and each axis was subdivided into at least 20 elements. Calcium was injected into the simulation as if all active channels were clustered together and took up an 8x8 $nm^2$ patch each (close to the tightest packing possible given their size). The top face was either reflective or clamped at starting concentrations (this made a negligible difference) and the sides were reflective (as if this were a unit cell repeated indefinitely). These conditions match the single-channel case when the cluster size is set to 1.

Immobile buffers made essentially no difference to the results; in the data presented here, simulations had 500 $\mu$M of an immobile calbindin-like buffer. The simulations are relatively insensitive to precise details of buffer kinetics; changing buffer kinetics by a factor of two produced similar results.

1. Baird, G.S., Zacharias, D.A. & Tsien, R.Y. Biochemistry, mutagenesis, and oligomerization of DsRed, a red fluorescent protein from coral. *Proc. Natl, Acad. Sci.* **97,** 11984-9 (2000).

2. Smith, G.D. Modeling local and global calcium signals using reaction-diffusion equations. In, computational neuroscience: realistic modeling for experimentalists, editor Schutter, E.D. p. 49-85 (CRC Press, Boca Raton Florida, 2001).